

# 1 Pleiotropic effects of *MORC2* derive from its epigenetic 2 signature

3 Fatemeh Peymani,<sup>1,2,†</sup> Tomohiro Ebihara,<sup>2,†</sup> Dmitrii Smirnov,<sup>1,2,†</sup> Robert Kopajtich,<sup>1,2</sup> Masahiro  
4 Ando,<sup>3</sup> Enrico Bertini,<sup>4</sup> Rosalba Carrozzo,<sup>5</sup> Daria Diodato,<sup>4</sup> Felix Distelmaier,<sup>6</sup> Fang Fang,<sup>7</sup>  
5 Daniele Ghezzi,<sup>8</sup> Maja Hempel,<sup>9,10</sup> Katarzyna Iwanicka-Pronicka,<sup>11</sup> Thomas Klopstock,<sup>12,13,14</sup>  
6 Sarah L. Stenton,<sup>1,2</sup> Costanza Lamperti,<sup>8</sup> Zhimei Liu,<sup>7</sup> Aysylu Murtazina,<sup>15</sup> Yuji Okamoto,<sup>3,16</sup>  
7 Yasushi Okazaki,<sup>17</sup> Dorota Piekutowska-Abramczuk,<sup>11</sup> Agn s R tig,<sup>18</sup> Oxana Ryzhkova,<sup>15</sup>  
8 Christian Schlein,<sup>19</sup> Olga Shagina,<sup>15</sup> Hiroshi Takashima,<sup>3</sup> Polina G. Tsygankova,<sup>15</sup> Michael  
9 Zech,<sup>1,2</sup> Thomas Meitinger,<sup>1</sup> Masaru Shimura,<sup>2,20</sup> Kei Murayama<sup>17,20,†</sup> and Holger Prokisch<sup>1,2,21,†</sup>

10 †These authors contributed equally to this work.

## 11 Abstract

12 Heterozygous missense mutations in *MORC2* have been implicated in various clinical entities,  
13 ranging from early-onset neurodevelopmental disorders to late-onset neuropathies. The  
14 mechanism underlying the phenotypic heterogeneity and pleiotropic effects of *MORC2* has  
15 remained elusive.

16 Here, we analyzed blood and fibroblast DNA methylation, transcriptomes, proteomes, and  
17 phenotypes of 53 *MORC2* patients.

18 We identified a *MORC2*-specific DNA methylation epsignature that is universal across all  
19 *MORC2*-associated phenotypes and conserved across different tissues. The *MORC2* epsignature  
20 consists mainly of DNA hypermethylation in promoter regions, leading to transcriptional  
21 repression of target genes resulting in a *MORC2*-specific RNA signature. Concomitant  
22 downregulation of three disease-associated genes *-ERCC8*, *NDUFAF2*, and *FKTN*- at different  
23 levels mirrors the variable biochemical defects and clinical manifestations observed in *MORC2*

  The Author(s) 2025. Published by Oxford University Press on behalf of the Guarantors of Brain. This is an Open Access article distributed under the terms of the Creative Commons Attribution-NonCommercial License (<https://creativecommons.org/licenses/by-nc/4.0/>), which permits non-commercial re-use, distribution, and reproduction in any medium, provided the original work is properly cited. For commercial re-use, please contact [reprints@oup.com](mailto:reprints@oup.com) for reprints and translation rights for reprints. All other permissions can be obtained through our RightsLink service via the Permissions link on the article page on our site—for further information please contact [journals.permissions@oup.com](mailto:journals.permissions@oup.com).

1 patients. Silencing of *NDUFAF2* accounts for the Leigh syndrome manifestation, whereas  
2 dysmorphic features are due to the repression of *ERCC8*.

3 Overall, we showed that pathogenic *MORC2* variants cause specific epigenature, whereby  
4 methylation level variability and its repression impact on target genes explains the pleiotropy and  
5 predicts phenotypic heterogeneity in *MORC2*-related disorders. We predict that epigenetic  
6 variation may underlie pleiotropy in other Mendelian disorders.

7

### 8 **Author affiliations:**

9 1 Institute of Human Genetics, School of Medicine and Health, Technical University of Munich,  
10 81675 Munich, Germany

11 2 Institute of Neurogenomics, Computational Health Center, Helmholtz Munich, 85764,  
12 Neuherberg, Germany

13 3 Department of Neurology and Geriatrics, Kagoshima University Graduate School of Medical  
14 and Dental Sciences, 890-8544 Kagoshima, Japan

15 4 Neuromuscular Disorders Research Unit, Bambino Gesù Children's Hospital IRCCS, 00165  
16 Rome, Italy

17 5 Laboratory of Medical Genetics, Translational Cytogenomics Research Unit, Bambino Gesù  
18 Children's Hospital, IRCCS, 00165 Rome, Italy

19 6 Department of General Pediatrics, Neonatology and Pediatric Cardiology, University Children's  
20 Hospital, Heinrich-Heine-University Düsseldorf, 40225 Düsseldorf, Germany

21 7 Department of Neurology, Beijing Children's Hospital, Capital Medical University, 100005  
22 Beijing, China

23 8 Unit of Medical Genetics and Neurogenetics, Fondazione IRCCS Istituto Neurologico Carlo  
24 Besta, 20133 Milano, Italy

25 9 Institute of Human Genetics, Heidelberg University, 69120 Heidelberg, Germany

26 10 Institute of Human Genetics, University Hospital Heidelberg, 69120 Heidelberg, Germany

- 1 11 Department of Medical Genetics, The Children's Memorial Health Institute, 04-730 Warsaw,  
2 Poland
- 3 12 Department of Neurology, Friedrich-Baur-Institute, LMU University Hospital, Ludwig-  
4 Maximilians-Universität (LMU) München, 81377 Munich, Germany
- 5 13 German Center for Neurodegenerative Diseases (DZNE), 81377 Munich, Germany
- 6 14 Munich Cluster for Systems Neurology (SyNergy), 81377 Munich, Germany
- 7 15 Research Centre for Medical Genetics, 115522 Moscow, Russia
- 8 16 Department of Physical Therapy, Kagoshima University of School of Health Sciences, 890-  
9 8544 Kagoshima, Japan
- 10 17 Diagnostics and Therapeutics of Intractable Diseases, Intractable Disease Research Center,  
11 Graduate School of Medicine, Juntendo University, 113-8421 Tokyo, Japan
- 12 18 UMR1163, Université Paris Descartes, Sorbonne Paris Cité, Institut Imagine, 75015 Paris,  
13 France
- 14 19 Institute of Human Genetics, University Medical Center Hamburg-Eppendorf, 20246 Hamburg,  
15 Germany
- 16 20 Department of Metabolism, Chiba Children's Hospital, 266-0007 Chiba City, Japan
- 17 21 German Center for Child and Adolescent Health (DZKJ), partner site Munich, 81377 Munich,  
18 Germany
- 19
- 20 Correspondence to: Dr Holger Prokisch
- 21 Institute of Neurogenomics, Helmholtz Munich
- 22 Deutsches Forschungszentrum für Gesundheit und Umwelt (GmbH)
- 23 Ingolstädter Landstraße 1
- 24 85764 Neuherberg, Germany
- 25 E-mail: [holger.prokisch@helmholtz-munich.de](mailto:holger.prokisch@helmholtz-munich.de)
- 26

1 **Running title:** Multi-omics analysis in MORC2 patients

2 **Keywords:** pleiotropy; MORC2; epismutation; multi-omics; Leigh syndrome; CMT

3

## 4 **Introduction**

5 Pleiotropy, the simultaneous presentation of different phenotypes due to variants in a single gene,  
6 and phenotypic heterogeneity are common, yet often unexplained, features of monogenic disorders  
7 <sup>1</sup>. *MORC2* (Microorchidia CW-type zinc finger protein 2)-related disorders are a prime example of  
8 this phenomenon. Heterozygous missense mutations in *MORC2* have been identified in association  
9 with a number of disorders, including Charcot-Marie-Tooth disease type 2Z (CMT2Z) <sup>2-4</sup>, spinal  
10 muscular atrophy (SMA) <sup>5</sup>, Leigh syndrome (LS), mitochondrial disease (MD) <sup>6,7</sup>, and Cockayne  
11 syndrome (CS) <sup>8</sup>. In another study, patients with *MORC2* pathogenic variants have been grouped  
12 under the umbrella term DIGFAN, which stands for developmental delay, impaired growth,  
13 dysmorphic facies, axonal neuropathy <sup>9</sup> (**Fig. 1** and Supplementary Table 1-2).

14 At the molecular level, *MORC2* encodes a DNA-dependent ATPase chromatin remodeler that  
15 functions both dependently and independently of the human silencing hub (HUSH) complex <sup>10,11</sup>.  
16 Within the HUSH complex, *MORC2* contributes to silencing the expression of the retroelements,  
17 thereby maintaining genome integrity. The HUSH complex regulates the deposition of the  
18 repressive epigenetic mark H3K9me3 (trimethylation of histone H3 at lysine 9) and recruits  
19 *MORC2* to mediate chromatin compaction <sup>10,12,13</sup>. Independent of the HUSH complex, *MORC2* is  
20 involved in gene silencing and facilitating DNA repair by modulating chromatin structure-  
21 chromatin compaction and decompaction <sup>13-15</sup>. Disease-causing variants in the ATPase module of  
22 *MORC2* result in its increased activity and hyper-repression of target genes <sup>9,10,12</sup>. However, the  
23 molecular mechanism linking increased *MORC2* activity to the wide range of associated  
24 phenotypes, including mitochondrial dysfunction, remains poorly understood. Furthermore, the  
25 gain-of-function pathomechanism, the highly variable phenotypes, and the lack of functional  
26 assays pose challenges for interpreting the pathogenicity of novel variants of uncertain significance  
27 (VUS) in the *MORC2* gene.

28 In order to investigate the pathomechanism underlying *MORC2* gain-of-function pathogenic  
29 variants, we performed a multi-omics analysis of blood and fibroblast samples from *MORC2*

1 patients. We discovered a *MORC2*-specific epismature that is conserved across tissues and  
2 consistent across all related phenotypes. This epismature not only serves as a functional assay for  
3 *MORC2* VUS but also identifies hitherto unknown *MORC2* targets. Hypermethylation of promoter  
4 regions in target genes resulted in gene repression at levels similar to those seen in Mendelian  
5 disorders. The concurrent repression of disease-associated genes - *ERCC8*, *NDUFAF2*, *FKTN* -  
6 underpins the observed pleiotropy in patients. Among the targets, the methylation level of the  
7 bidirectional promoter of *ERCC8-NDUFAF2* exhibits the strongest correlation with disease  
8 severity, being higher in LS than in CMT. Overall, our study illustrates the link between epigenetic  
9 modifications and pleiotropy in Mendelian disorders.

## 10 **Materials and methods**

### 11 **Study cohort**

12 A cohort of 53 *MORC2* genetically diagnosed patients has been collected through both national  
13 sources and international collaborations. The cohort includes 39 newly identified cases and 14  
14 previously reported ones<sup>3,6</sup>. Patient phenotypes were extracted and coded as Human Phenotype  
15 Ontology (HPO) terms (Supplementary Table 2). Written informed consent was obtained from all  
16 individuals or their guardians prior to evaluation and testing, in accordance with the Declaration  
17 of Helsinki, and approved by the ethical committees of the participating centers.

18 The classification of disease types for unreported cases was performed as follows. Initially, cases  
19 with developmental delay and bilateral basal ganglia or brainstem lesions on head MRI were  
20 classified as Leigh syndrome. Subsequently, cases with multisystem symptoms involving more  
21 than three organs and with defects in mitochondrial oxidative phosphorylation enzymes or elevated  
22 lactate were classified as MD<sup>16</sup>. Among the remaining cases, those with growth impairment (short  
23 stature, microcephaly) and characteristic facial features were classified as Cockayne syndrome<sup>17</sup>.  
24 Cases not classified into the above three categories were characterized by predominant peripheral  
25 neuropathy and were classified as CMT (Supplementary Table 1-2).

26 A clinical-radiological score<sup>18</sup> was calculated to evaluate the clinical similarity of the cases to  
27 Cockayne syndrome. Clinical symptoms were aggregated for all patients; however, head imaging

1 was omitted in cases where central nervous system symptoms were not the primary manifestation  
2 (Supplementary Table 2).

3 DNA methylation profiling was performed on both blood and fibroblasts in 45 patients, depending  
4 on material availability. One patient had both blood and fibroblasts, and one patient had two  
5 samples from different time points, resulting in 47 DNA methylation data from *MORC2* patients  
6 ( $n = 35$  blood and  $n = 12$  fibroblast DNA methylation)

7 RNA-seq and proteomics were performed on fibroblasts from 12 and 13 *MORC2* patients,  
8 respectively.

## 9 **DNA methylation analysis pipeline**

### 10 **Processing of DNA methylation**

11 Genomic DNA was extracted from blood and fibroblast samples. DNA methylation analysis was  
12 performed on bisulfite-converted DNA from both blood and fibroblast samples using the Infinium  
13 Methylation EPIC v1.0 and v2.0 BeadChip arrays, in accordance with the manufacturer's protocols  
14 at Helmholtz Munich Core Facility. DNA methylation data preprocessing was performed using  
15 the minfi package<sup>19</sup> in R version 4.3.1. Initial quality control involved filtering out samples based  
16 on several criteria: average detection  $p$ -value less than 0.05, discordance in recorded gender and  
17 predicted gender based on the methylation profile, methylation intensity deviating more than three  
18 standard deviations from the mean, and non-bimodal distribution in density plots. Quantile  
19 normalization was applied on the CpG sites common between EPIC v1.0 and EPIC v2.0 arrays. In  
20 addition, the probes with a detection  $p$ -value greater than 0.01, probes overlapping with SNPs,  
21 cross-reactive probes, and probes located on the X and Y chromosomes were excluded from the  
22 analysis. Following these filtering criteria, 631,142 CpG sites in 512 samples ( $n = 481$  blood and  
23  $n = 31$  fibroblast) remained for downstream analysis. Methylation Beta values and M-values were  
24 calculated for all the CpG sites. The proportions of white blood cell types were estimated using  
25 the Houseman method<sup>20</sup>. Age was also inferred from methylation data using the Horvath method  
26 implemented in the methylclock package<sup>21</sup>.

## 1 **Discovery of *MORC2*-specific episignature**

2 Epigenome-wide association study (EWAS) was performed on blood DNA methylation. A cohort  
3 of 13 *MORC2* patients and 58 healthy controls were selected, and 80:20 percent train-to-test  
4 splitting was performed. EWAS was conducted on the training cohort consisting of 10 *MORC2*  
5 patients and 46 healthy controls. Linear regression on the methylation values (M-values), adjusting  
6 for disease status (*MORC2* vs. control), age, gender, white blood cell type composition, and the  
7 version of the EPIC array (EPIC v1.0 and v2.0) was performed using the limma package. CpG  
8 sites showing significant differences at Bonferroni adjusted  $p$ -values  $< 0.05$  were considered as  
9 differentially methylated positions (DMPs).

10 Given the extensive number of CpG sites showing significant differences at Bonferroni-adjusted  
11  $p$ -values  $< 0.05$  ( $n = 760$  CpG), we employed several criteria to refine the selection of CpG sites  
12 for inclusion in our diagnostic classifier. Following the approach by Levy *et al.*<sup>22</sup> we computed a  
13 methylation score for each site by multiplying the negative log-transformed false discovery rate  
14 (FDR) by the absolute value of the log-fold change (logFC). The top 1000 probes, ranked by this  
15 score, were initially selected. The feature importance for the selected CpGs was calculated using  
16 the filterVarImp function from the Caret package. From this analysis, 220 CpG sites exhibiting an  
17 area under the curve (AUC) greater than 0.99 were chosen for training the classifier.

18 Unsupervised visualization was performed by calculating the Euclidean distances between  
19 samples, followed by multidimensional scaling (MDS) on the M-values of 220 CpG sites to  
20 examine the data structure and clustering of *MORC2* patients and controls. Subsequently, a support  
21 vector machine (SVM) classifier was trained using the e1071 package based on the M-values of  
22 the same 220 CpG sites. The training was performed on the samples used for the EWAS analysis.  
23 A 10-fold cross-validation with a linear kernel was applied. The probability scores generated by  
24 the classifier were used to classify *MORC2* patients, with a threshold set at a score greater than  
25 0.5. The classifier was tested on a blood sample cohort comprising three *MORC2* patients, 12  
26 healthy controls, and 368 samples with other genetic disorders, and on a fibroblast sample cohort  
27 consisting of six *MORC2* patients and 18 healthy or diseased controls. In addition, the phenotype  
28 specificity of the classifier was evaluated in a validation cohort of 49 DNA methylation samples  
29 collected after the discovery of episignature, including 28 samples from *MORC2* patients ( $n = 22$   
30 blood;  $n = 6$  fibroblast DNA methylation), 22 of whom were clinically diagnosed with CMT.

## 1 **Discovery of phenotype-specific epsignature**

2 A total of 43 samples from *MORC2* patients exhibiting the *MORC2*-specific epsignature were  
3 clinically diagnosed with LS ( $n = 13$ ), MD ( $n = 6$ ), or CMT ( $n = 24$ ). For the EWAS, data from  
4 the two most distinct phenotypes, typical CMT and LS, were selected. DNA methylation data for  
5 the majority of LS patients ( $n = 10$ ) were derived from fibroblasts, whereas for CMT patients, the  
6 data were obtained mainly from blood samples ( $n = 23$ ). To mitigate the confounding effect of  
7 tissue in EWAS, we combined the DNA methylation data of CMT patients with fibroblast DNA  
8 methylation of control cell lines. EWAS was performed comparing 10 LS patients against 32  
9 samples comprising 16 CMT patients and 16 controls. Gender, age, tissue (blood or fibroblast),  
10 and the version of the EPIC array were included as covariates. CpG sites at Bonferroni-adjusted  
11  $p$ -values  $< 0.05$  ( $n = 80$  CpG sites) were considered significant.

12 Similar to the discovery of the epsignature, the MDS plot was utilized to visualize the data  
13 structure using the 80 CpG sites identified in the previous step. Subsequently, the SVM classifier  
14 was trained on the set of samples used for EWAS, employing 5-fold cross-validation to classify  
15 *MORC2* patients with LS/MD versus those with CMT. The classifier was tested on additional  
16 samples, including nine patients with LS/MD and 11 patients with CMT. The classifier was further  
17 tested on DNA methylation of a cohort of 449 samples ( $n = 3$  fibroblast and  $n = 446$  blood).

## 18 **Annotation of DNA methylation CpG sites**

19 CpG site annotation was performed using the `getAnnotation` function from the  
20 `IlluminaHumanMethylationEPICanno.ilm10b4.hg19` package in R. The spatial localization of  
21 CpG sites relative to genes was determined using the “UCSC\_RefGene\_Group” column, which  
22 includes TSS1500 (200-1500 bases upstream of the TSS), TSS200 (0-200 bases upstream of the  
23 TSS), 5’UTR, 1st exon, ExonBnd (exon boundaries), Body (gene body), and 3’UTR. We defined  
24 the gene promoters as CpGs located in TSS1500 or TSS200. Since each CpG site can have multiple  
25 annotations based on its location relative to different transcripts of the gene, we considered the  
26 most frequent annotation for downstream analysis to ensure one annotation per CpG. We also  
27 repeated the analysis using all possible annotations for each CpG, but this did not show significant  
28 differences compared to the first analysis.

1 Gene annotations were obtained from the InfiniumAnnotation database  
2 ([https://zwdzwd.github.io/InfiniumAnnotation/EPIC\\_hm450\\_hg19.html](https://zwdzwd.github.io/InfiniumAnnotation/EPIC_hm450_hg19.html)), which map the genes to  
3 the CpG sites spanning from 1.5 kb upstream of the transcription start site to the transcription  
4 termination site, using GENECODE release 26. For CpG sites with multiple corresponding genes,  
5 all genes were considered for the analysis.

6 HUSH target sites and MORC2 binding sites were obtained from Seczynska *et al.*<sup>23</sup> and  
7 Tchasovnikarova *et al.*<sup>10</sup>, respectively. The CpGs located within the identified loci were marked  
8 as CpGs in the HUSH target site or MORC2 binding site.

### 9 **Sample-based aggregated methylation value**

10 The calculation of the methylation value for each sample based on a set of CpG sites was  
11 performed as follows. First, for each CpG, we calculated the methylation Z-score by subtracting  
12 the mean M-value across all DNA methylation samples from the M-value of that CpG in each  
13 sample and dividing by the standard deviation. Then, for each sample, we calculated the mean of  
14 the methylation Z-scores for the specific set of CpG sites (such as the 220 CpGs in the episignature  
15 or the 3,019 CpGs mapped to HUSH targets).

### 16 **Transcriptome analysis pipeline**

#### 17 **RNA sequencing and Data Processing**

18 RNA sequencing was performed according to <sup>24,25</sup>. Briefly, RNA was isolated from patient-derived  
19 skin fibroblasts, and library preparation was conducted using either the TruSeq Stranded mRNA  
20 or Illumina Stranded mRNA Ligation protocol. The RNA libraries were sequenced as 100 bp  
21 paired-end runs on Illumina HiSeq2500 or HiSeq4000 platforms. RNA-seq reads were  
22 demultiplexed and aligned to the hg19 genome assembly (UCSC Genome Browser build) using  
23 STAR version 2.7.0a. The DROP pipeline (version 1.3.4) was employed for read counting and  
24 quality control, using the GRCh37 primary assembly, release 29, of the GENCODE project as the  
25 reference genome. RNA-SEQC was utilized for quality control, and the summarizeOverlaps  
26 function from the GenomicAlignments R package was used to count reads. Genes with a 95th  
27 percentile FPKM below one were filtered out as not sufficiently expressed.

## 1 **Discovery of *MORC2*-specific RNA-signature**

2 64 samples, comprising 12 *MORC2* samples, 18 healthy controls, and 34 diseased controls, were  
3 selected for differential expression analysis. An 80:20 train-test split was performed on this cohort,  
4 resulting in a training set of 10 *MORC2* patients and 42 controls (13 healthy and 29 diseased),  
5 which was used for the identification of differentially expressed genes (DEGs). Principal  
6 Component Analysis (PCA) was conducted and revealed the impact of library preparation  
7 protocols.

8 DESeq2 version 1.34.0 was employed for the normalization and detection of DEGs. Briefly,  
9 DESeq2 estimates size factors to normalize for differences in sequencing depth across samples. A  
10 design formula incorporating disease status (*MORC2* vs. others), sex, and library protocol was  
11 used to model the count data using negative binomial generalized linear models (GLMs). The  
12 Wald test was applied to assess significant differences in gene expression between *MORC2*  
13 patients and controls while accounting for the effects of covariates. A threshold of BH-adjusted  $p$ -  
14 value  $< 0.05$  was used to determine statistically significant differentially expressed genes ( $n = 106$   
15 DEGs). Unsupervised clustering was performed on 106 DEGs, in the same way as performed for  
16 episignature, to examine the clusterization of *MORC2* patients and control samples.

17 An SVM classifier was trained on 106 DEGs using a methodology analogous to that employed for  
18 DNA methylation. The classifier was trained on normalized counts, where normalization was  
19 performed using DESeq2 by estimating size factors with the estimateSizeFactors function and  
20 applying variance stabilizing transformation (VST) with the vst function to stabilize the variance  
21 across the data, followed by scaling. The classifier was trained on the sample set used for DEGs  
22 detection with 10-fold cross-validation. The SVM probability scores were utilized similarly to the  
23 DNA methylation analysis, with a threshold of 0.5 set to classify *MORC2* patients. The classifier  
24 was tested on the test cohort of two *MORC2* patients and ten healthy or diseased controls, as well  
25 as an additional set of 168 genetically undiagnosed samples.

## 26 **Detection of expression outliers**

27 Expression outliers were identified using the OUTRIDER package on the transcriptome of  
28 fibroblast cell lines of a cohort of 877 individuals consisting of 12 *MORC2* patients. OUTRIDER  
29 employs a denoising autoencoder to control for latent effects and provides an RNA z-score for

1 each gene and sample, allowing for the detection of expression outliers. Unsupervised clustering  
2 has also been performed on the denoising autoencoder-derived normalized counts of 106 DEGs.

### 3 **Proteomics analysis pipeline**

4 Proteomics has been performed on fibroblast cell lines of 660 samples consisting of 13 *MORC2*  
5 patients, as described by Kopajtich *et al.*<sup>26</sup>. In summary, the protocol included reduction,  
6 alkylation, tryptic digestion using Trypsin Gold (Promega), and TMT labeling and liquid  
7 chromatography-mass spectrometry measurements. In total, 9040 proteins have been detected. The  
8 proteins with missing values in more than 20 percent of the samples were filtered out, resulting in  
9 6749 proteins. PROTRIDER<sup>26</sup> has been utilized for normalization and protein outlier detection.  
10 Similar to OUTRIDER, PROTRIDER employed a denoising autoencoder to mitigate the influence  
11 of latent confounders. Proteins with a Z-score < -2 were classified as protein outliers. Recurrent  
12 protein outliers were defined as those identified as outliers in at least two *MORC2* patients. The  
13 significance of recurrent protein outliers in *MORC2* patients was assessed using a one-sided Fisher  
14 exact test.

15 Cryo-EM structure in the active state (PDB ID: 6G2J) was used in PyMol V.2.5.4 (Schrödinger)  
16 to visualize the protein abundances in respiratory chain complex I.

### 17 **Oxygen Consumption Rate (OCR) measurement**

18 OCR was examined using skin fibroblasts according to the method previously described<sup>27</sup>. For  
19 each disease type and control (NHDF), 22 to 24 wells were used, and the measurement was  
20 conducted twice.

## 21 **Results**

### 22 **Discovery of tissue-independent *MORC2* episignature**

23 Pathogenic variants in genes involved in the epigenetic machinery have been shown to result in  
24 gene-specific methylation changes called episignatures. These episignatures serve as highly  
25 sensitive and specific biomarkers that can be used as functional assays to assess the functional  
26 impact of VUS in a growing number of Mendelian disorders<sup>22</sup>. Despite *MORC2*'s recognized role  
27 in gene regulation, its genome-wide impact on DNA methylation remains unexplored. To assess

1 the impact of pathogenic variants in *MORC2* on DNA methylation, we conducted an epigenome-  
2 wide association study (EWAS) using 10 *MORC2* patients and 46 healthy controls (Supplementary  
3 Table 3). The analysis identified 760 differentially methylated positions (DMPs) when corrected  
4 for multiple testing (Bonferroni p-adjusted value  $< 0.05$ ); 93% ( $n = 707$ ) were hypermethylated in  
5 *MORC2* patients (**Fig. 2A** and Supplementary Table 4). The 760 DMPs were mapped to 480 genes  
6 (differentially methylated genes; DMGs). From these 760 DMPs, we selected the 220 most  
7 differentiating CpG sites (see Methods for details) for unsupervised analysis. This resulted in a  
8 clear separation between *MORC2* patients and controls (**Extended Fig. 1A**). To validate the  
9 specificity of the identified epismature, we trained a support vector machine (SVM) classifier on  
10 blood DNA methylation data using 220 CpGs on the sample set used in EWAS. This classifier  
11 was then tested on an independent cohort of three *MORC2* patients, 12 healthy controls, 281  
12 patients with mitochondrial disease, and 86 patients with other neurodevelopmental disorders. The  
13 classifier successfully identified all *MORC2* patients in the test set (**Fig. 2C**).

14 DNA methylation patterns vary significantly across tissues. To date, DNA methylation  
15 epismatures have been identified and applied in diagnostics on blood samples. However, blood  
16 is often not the most suitable tissue for functional studies, whereas fibroblasts are well-established  
17 in diagnostic routines for pathomechanistic investigations. We sought to evaluate if the *MORC2*-  
18 specific epismature found in blood could be detected across different tissues. Therefore, we tested  
19 the classifier on DNA methylation data from 24 fibroblast cell lines, including six from *MORC2*  
20 patients. All the *MORC2* patients were successfully classified, as with the blood samples (**Fig.**  
21 **2C**). This finding demonstrates that the disease-specific methylation changes that build the  
22 epismature are conserved across different tissues and stronger than tissue-dependent differences.

23 Since the classifier was solely tested on *MORC2* patients with MD, we sought to evaluate its  
24 phenotype specificity. We further collected 28 samples from *MORC2* patients, including 22 with  
25 a CMT phenotype and 21 additional disease controls, including one patient with a benign missense  
26 variant in *MORC2*. All groups were correctly classified except for 3 *MORC2* CMT patients that  
27 were falsely classified as controls (Area Under the Curve, AUC = 0.988) (**Fig. 2C**). Even though  
28 the probability from the classifier was a little bit elevated, it was still in the benign range. All the  
29 variants reported in these three patients are located in the transducer S5-like domain, representing  
30 3 out of 7 variants in this domain that did not show the epismature. Further investigation is needed

1 to clarify the pathogenicity of these variants. Overall, we demonstrated that the epesignature is  
2 universal for all *MORC2*-related disorders investigated.

3 Leveraging on the high specificity of the *MORC2* epesignature, we tested the classifier on the DNA  
4 methylation profile of an MD patient carrying a VUS in *MORC2* (NM\_001303256.3: c.535C>T,  
5 p.Arg179Cys), classified according to the ACMG/AMP guidelines. The variant is located in the  
6 hotspot region of the ATPase module. The classifier showed a clear benign result, which was later  
7 supported by segregation analysis showing the presence of the variant in the healthy, unaffected  
8 mother. We concluded that this variant is not a significant contributor to the observed disease  
9 phenotype and reclassified it as benign (**Fig. 2C**).

10 To date, all pathogenic variants reported in *MORC2* are exclusively missense variants, with a  
11 suspected gain-of-function mechanism<sup>10,12</sup>. To verify this hypothesis, we assessed the impact of a  
12 heterozygous stop-gain variant (NM\_001303256.3: c.268C>T, p.Arg90Ter) in *MORC2* in an  
13 individual with an unrelated phenotype of hypertension. The classifier correctly predicted this  
14 variant to be benign, supporting the hypothesis that gain-of-function, not loss-of-function (LOF),  
15 is the pathomechanism of pathogenic *MORC2* variants (**Fig. 2B-C**).

## 16 **Predominant localization of *MORC2* epesignature in gene promoters**

17 Currently, the primary motivation to search for epesignatures and the value of an identified  
18 epesignature lies in its potential for functional validation of VUS and its impact on subsequent  
19 variant classification. However, the disease-specific methylation changes have broadly failed to  
20 provide further insights into the Mendelian disease pathomechanisms. To explore *MORC2*  
21 pathomechanism, we analyzed the spatial distribution of DMPs in the genome. In a previous study  
22 by Tchasovnikarova *et al.*<sup>10</sup>, *MORC2* binding sites were identified and found to be enriched at  
23 transcription start sites (TSSs) and HUSH targets. Indeed, we observed a significant enrichment  
24 of DMPs in *MORC2* binding sites<sup>10</sup> and gene promoter regions, as well as HUSH target sites<sup>23</sup>  
25 (**Fig. 2D**). Of the DMPs located at *MORC2* binding sites (23%), 60% are located in gene promoter  
26 regions and 14% overlapped with HUSH target sites (**Fig. 2E**). This observation aligns with  
27 previous studies indicating that *MORC2* binding sites are mainly located at TSSs and, to a lesser  
28 extent, at HUSH target loci within gene bodies<sup>10</sup>. Moreover, among the DMPs that do not overlap  
29 with known *MORC2* target sites, 30% are also located in gene promoter regions, while 10%  
30 overlap with HUSH target sites. (**Fig. 2D-E**). Overall, this suggests that although some of the

1 effects of mutant MORC2 on DNA methylation are mediated through interactions with the HUSH  
2 complex, the majority are driven by the HUSH-independent function of MORC2.

3 Around 60% of hypermethylation sites have not been previously identified either as MORC2  
4 targets or HUSH targets. This could represent unrecognized physiological targets of MORC2 or  
5 novel targets arising as a result of *MORC2* gain-of-function variants. To differentiate between the  
6 two alternatives, we took advantage of the *MORC2* LOF. We hypothesized that physiological  
7 targets of MORC2 should show a reduced level of methylation in the carrier of the LOF variant.  
8 Indeed, across all known HUSH target sites, the LOF variant in *MORC2* resulted in reduced  
9 methylation. This pattern is even more pronounced in the newly identified sites. While DMPs are  
10 hypermethylated in *MORC2* patients, they are hypomethylated in the heterozygous LOF variant  
11 carrier (**Extended Fig. 2**). Taken together, these data support the idea that increased methylation  
12 occurs mostly at MORC2 physiological targets rather than at novel binding sites arising from gain-  
13 of-function mutations.

14 Overall, our analysis demonstrates that the CpGs comprising the *MORC2* episcapature are  
15 predominantly located in gene promoters, and the comparison of *MORC2* gain-of-function and  
16 LOF variants further extends the list of previously identified MORC2 targets.

## 17 **MORC2 mutants drive specific gene repression, resulting in an** 18 **RNA-signature**

19 Building on the observation that *MORC2* mutations induce DNA hypermethylation in gene  
20 promoters, we next explored the functional impact of this promoter hypermethylation on gene  
21 expression, leveraging the conserved episcapature in fibroblast cell lines. Differential expression  
22 analysis of 10 *MORC2* patients and 42 control cell lines revealed 106 differentially expressed  
23 genes (DEGs) at FDR-adjusted  $p$ -value  $< 0.05$  (**Fig. 3A** and Supplementary Table 5-6). Notably,  
24 97% of these genes (103 out of 106) were downregulated, and nearly half exhibited a significant  
25 increase in promoter methylation, consistent with the concept that hypermethylation in promoter  
26 regions results in the silencing of gene expression. Furthermore, these promoter regions were also  
27 hypermethylated in blood samples, suggesting an early establishment of MORC2 gain-of-function  
28 specific methylation changes in patients.

1 We then asked whether the differentially expressed genes (DEGs) were specific and sensitive  
2 enough to classify *MORC2* patients. Using the same approach as for epismature discovery, we  
3 applied an unsupervised analysis on both DESeq2-normalised (size factor normalization followed  
4 by variance stabilizing transformation) and OUTRIDER-normalised (employing denoising  
5 autoencoder)<sup>28</sup> counts of 106 DEGs. A separation between *MORC2* patients and controls was  
6 observed, with the separation being more distinct when using OUTRIDER-normalized counts  
7 (**Extended Fig. 1B,C**). Subsequently, we trained an SVM classifier on the same set of samples  
8 and tested it on an independent cohort of 180 samples (two *MORC2* patients, 10 healthy or disease  
9 controls, and 168 genetically undiagnosed patients). The classifier successfully distinguished the  
10 *MORC2* patients from all other samples (**Fig. 3B**). In conclusion, heterozygous pathogenic variants  
11 in *MORC2* result in a hyperactive enzyme that causes promoter hypermethylation of *MORC2*  
12 targets, leading to the silencing of a defined set of genes. This effect is strong and specific enough  
13 to establish an RNA-based *MORC2* classifier.

## 14 **MORC2 downstream targets provide mechanistic insight into the** 15 **pleiotropy of *MORC2***

16 Having identified *MORC2*-specific dysregulated genes, we questioned whether these targets share  
17 common features. Gene set enrichment analysis revealed a significant overrepresentation of C2H2-  
18 type zinc finger (ZNF) genes among both DMGs and DEGs, with C2H2-ZNF genes comprising  
19 43% of the DEGs ( $n = 47$ ) (**Fig. 4**). As a proof of concept, ZNF genes have been previously shown  
20 to be silenced in *MORC2* mutant cell lines. However, the repression has been attributed to histone  
21 methylation (H3K9me3) via the HUSH-MORC2 complex<sup>10,13,29</sup>. Our data showed that promoter  
22 hypermethylation of ZNF genes also contributes to their transcriptional repression. Despite this  
23 enrichment, none of the dysregulated C2H2-ZNF genes identified in our study have been  
24 associated with a genetic disorder.

25 We next asked whether the dysregulated genes at both methylation and expression levels have  
26 been associated with Mendelian disorders. Four disease-associated genes - *ERCC8*, *NDUFAF2*,  
27 *FKTN*, and *NHLRC1* - were identified (**Extended Fig. 3A**). Notably, two of these genes, *ERCC8*  
28 and *NDUFAF2*, share the same bidirectional promoter. Three of the four genes - *ERCC8*,  
29 *NDUFAF2*, and *FKTN* - were also identified as recurrent expression outliers in *MORC2* patients,

1 with reduced expression levels typical of monogenic disorders caused by primary mutations in  
2 these genes (**Fig. 5A-D**).

3 To further validate the low expression level of the dysregulated disease genes, we performed  
4 proteomics on 13 fibroblast cell lines of *MORC2* patients. While *ERCC8* and *FKTN* proteins were  
5 not detected in our proteomics assay, *NDUFAF2* was detected and found as a recurrent protein  
6 outlier (**Fig. 5C**). The level of *NDUFAF2* protein in *MORC2* patients fibroblasts was as low as in  
7 patients with pathogenic variants in *NDUFAF2* itself (Protein Z-score < -2).

8 *NDUFAF2* encodes a mitochondrial respiratory chain complex I (CI) assembly factor that  
9 facilitates the last step of CI assembly, integrating the N module into CI. Pathogenic variants in  
10 *NDUFAF2* have previously been reported in patients with MD and LS and decreased CI levels and  
11 activity<sup>30-32</sup>. In addition to the reduced level of *NDUFAF2*, our proteomics data also show a  
12 significant reduction of CI N- and Q-module proteins, although their RNA expression is within  
13 the normal physiological range (**Fig. 5C** and Supplementary Table 7). This finding underscores  
14 the functional downstream effect of the *NDUFAF2* dysfunction. Overall, the reduced level of  
15 *NDUFAF2* and the consequent impairment of respiratory chain CI establish a functional link  
16 between *MORC2* mutations and mitochondrial dysfunction and explain the clinical presentation  
17 of LS.

18 Biallelic pathogenic variants in *ERCC8*, mostly LOF variants, have been reported in patients with  
19 Cockayne syndrome<sup>33,34</sup>, another phenotype observed in *MORC2* patients<sup>8</sup>. *ERCC8* encodes a  
20 WD repeat protein known as Cockayne syndrome A protein (CSA), which plays a role in DNA  
21 damage repair<sup>35</sup>. Accumulation of DNA damage has been observed in *Morc2a* mutant mice and  
22 has remained so far unexplained<sup>36</sup>. We conclude that the reduced expression of *ERCC8* contributes  
23 to the CS features observed in *MORC2* patients, including signs of accelerated aging.

24 *FKTN*, another dysregulated gene, encodes fukutin, an enzyme involved in the glycosylation of  $\alpha$ -  
25 dystroglycan. Biallelic pathogenic variants in *FKTN* are associated with dystroglycanopathies, a  
26 spectrum of muscular dystrophies that can also be accompanied by brain and eye malformations  
27 as well as cardiomyopathy<sup>37,38</sup>. Muscular dystrophy has been reported in *MORC2* patients, and  
28 some have shown elevated serum creatine kinase levels, a biomarker of muscle damage<sup>9,39</sup>.  
29 Nevertheless, cobblestone lissencephaly, a hallmark feature of *FKTN*-related disorders on brain  
30 MRI, has not been observed so far in *MORC2* patients. Our findings suggest that *FKTN*

1 downregulation may contribute to the muscular dystrophy observed in *MORC2* patients.  
2 Additionally, we suggest that *MORC2* variants be considered in patients presenting with *FKTN*-  
3 specific brain abnormalities.

4 While mitochondrial CI deficiency was the predominant biochemical defect observed in *MORC2*  
5 patients, complex II (CII) deficiency was occasionally noted. In agreement with this, we observed  
6 promoter hypermethylation and reduced expression of *SDHAF4*, a CII assembly factor, in two  
7 patients with CII deficiency (**Fig. 5E**). This observation highlights the variability of *MORC2*  
8 targets among patients, as evidenced in this case, leading to CII deficiency in a small subset of  
9 individuals.

10 Additionally, we observed a significant downregulation of *MORC2* itself, independent of any  
11 significant changes in DNA methylation (**Extended Fig. 3B**). Previous studies have identified  
12 *MORC2* as a target of the HUSH complex, with its downregulation observed in *MORC2* mutant  
13 cell line <sup>10</sup>. Our findings align with previous findings, supporting the hypothesis that the reduced  
14 *MORC2* expression is likely mediated by histone methylation (H3K9me3) via the HUSH complex  
15 rather than through DNA methylation.

16 Finally, we observed only marginal promoter hypermethylation and reduced expression of the  
17 *NHLRC1* gene. The gene was not identified as an expression outlier (**Extended Fig. 3C**). The  
18 pathogenic variants in *NHLRC1* have been associated with myoclonus epilepsy, a phenotype not  
19 observed in our cohort but previously reported in some *MORC2* patients <sup>9</sup>. Further investigation  
20 of *NHLRC1* promoter methylation in those patients is warranted.

## 21 **The level of methylation predicts phenotypic differences in *MORC2*-** 22 **related disorders**

23 *MORC2* patients present with overlapping symptoms of different disorders. Besides MRI findings  
24 which are specific to LS, all other symptoms are observed in subsets of both CMT and MD *MORC2*  
25 patients (**Fig. 6A** and Supplementary Table 1). Our integrative multi-omics analysis identified the  
26 key genes driving the *MORC2*-related phenotypes, highlighting their composite nature. The  
27 *MORC2*-related disorder is the consequence of variable quantitative gene silencing of at least three  
28 genes - *NDUFAF2*, *ERCC8*, *FKTN* - alongside additional genes that are affected in some but not  
29 all patients. How much does the genotype affect the variability? Generally, there is some

1 correlation between genotype and phenotype. Variants in the N-terminal GHKL domain are more  
2 frequently associated with severe neurodevelopmental disorders and MD, while those in the C-  
3 terminal GHKL domain and transducer-like domain are more commonly linked to CMT. However,  
4 several variants have been reported in association with variable clinical presentation, even among  
5 members of the same family (**Fig. 1C** and Supplementary Table 1) <sup>40</sup>.

6 We therefore asked whether the methylation pattern may help in predicting patient phenotypes.  
7 We selected patients from the two most distinct *MORC2*-related disorders, patients with LS ( $n =$   
8 10) from the MD cohort and patients with the typical presentation of CMT ( $n = 16$ ), as well as 16  
9 controls for differential methylation analysis (see Methods for details) and identified 80 DMPs at  
10 a Bonferroni-adjusted  $p$ -value  $< 0.05$  (Supplementary Table 3-4). Notably, 88% of the 80 DMPs  
11 had already been identified as *MORC2*-specific DMPs. An MDS plot using these 80 DMPs showed  
12 a clear separation between *MORC2* patients and controls in the first dimension. The second  
13 dimension separated *MORC2* patients with CMT from those with MD (**Fig. 6B**, **Extended Fig.**  
14 **4C**). A classifier was trained to predict the phenotypes and tested on an independent *MORC2*  
15 cohort, including 11 patients with CMT and 9 with MD, achieving high accuracy with an AUC of  
16 0.99 (**Extended Fig. 4A, B**). The classifier correctly predicted the phenotypes of two pairs of  
17 patients with the same affected amino acid but different LS and CMT phenotypes (**Extended Fig.**  
18 **4A**). This finding suggests that DNA methylation adds information on top of the genetic variant  
19 in predicting the patient phenotype. Given that *MORC2*-related disorders exist as a continuum  
20 (**Fig. 6A**), we recommend interpreting the phenotype-classifier results as probabilities indicating  
21 whether the clinical presentation is more characteristic of MD rather than CMT.

22 Among the identified DMPs, a significant proportion (16%) were located in the *ERCC8-*  
23 *NDUFAF2* bidirectional promoter. MD patients exhibited significantly higher methylation levels  
24 than those with CMT, while CMT patients still demonstrated significantly elevated methylation  
25 levels relative to controls (**Fig. 6C**). These findings suggest that mitochondrial dysfunction is also  
26 present in CMT patients. When comparing mitochondrial respiration, the fibroblast cell line from  
27 a CMT patient exhibited an intermediate phenotype, falling between that of an LS patient with CI  
28 deficiency and a healthy control (panel right of **Fig. 5C**).

29 We further investigated whether methylation levels across all DMPs were elevated in *MORC2*  
30 patients with MD compared to CMT. No significant differences in methylation levels were

1 observed between phenotypes when considering all *MORC2*-specific DMPs. While a significant  
2 increase in DNA methylation was observed in MD patients across the 80 phenotype-specific  
3 DMPs, the elevation was more pronounced at CpGs within the *ERCC8-NDUFAF2* promoter (**Fig.**  
4 **6D**). This suggests that methylation at this promoter plays a pivotal role in driving the phenotypic  
5 heterogeneity in *MORC2*-related disorders.

## 6 **Discussion**

7 DNA methylation epigenatures are increasingly recognized as specific biomarkers for a subset of  
8 rare disorders<sup>41</sup>. However, their application has so far been predominantly limited to diagnostic  
9 biomarkers, with minimal use in understanding disease pathomechanisms. In this study, we  
10 demonstrate that patients with pathogenic gain-of-function variants in *MORC2* share a common  
11 DNA methylation pattern despite displaying varied biochemical defects and broad clinical  
12 presentations. Strikingly, promoter hypermethylation of the target genes, which constitutes the  
13 core of the epigenature, is conserved across tissues and results in reduced RNA expression and  
14 protein levels with an effect size comparable to the Mendelian disorders due to pathogenic variants  
15 impacting the target genes themselves. The repression of known disease-associated genes and the  
16 degree of their downregulation explain the pleiotropy seen in *MORC2* patients. These *MORC2*-  
17 specific methylation changes further extend our knowledge of the molecular function of *MORC2*  
18 and its downstream targets.

19 *MORC2* patients have been so far classified into distinct disorders, such as CMT, SMA, CS, LS,  
20 and MD, based on their predominant symptoms. However, the phenotypic presentation is broader  
21 than these classifications, with overlapping features of different disorders that blur the boundaries  
22 between categories. Sacoto *et al.*<sup>9</sup> attempted to address the phenotypic variability by proposing a  
23 broad category named DIGFAN encompassing all *MORC2*-related disorders except CMT.  
24 However, patients rarely present with the full spectrum of DIGFAN features, and diagnosis  
25 remains reliant on identifying the underlying genetic cause in *MORC2*. In this study, we  
26 demonstrated that the composite repression of multiple disease-associated genes driven by  
27 *MORC2* hyperactivity underlies its pleiotropic effects. The variability in target genes and the level  
28 of repression amongst affected individuals account for the observed phenotypic heterogeneity,  
29 even in patients with the same mutation. A consistent observation across patients is impaired  
30 energy metabolism driven by mitochondrial CI deficiency. These results suggest that *MORC2*-

1 related disorders exist along a spectrum, ranging from mild CMT to severe LS. We propose  
2 moving away from splitting *MORC2*-related disorders into separate categories and instead lumping  
3 them into a single disease spectrum with a shared pathomechanism.

4 All *MORC2* patients diagnosed with an MD or LS had an age of onset within the first two years  
5 of life, which is also reported for all *NDUFAF2* patients. Neurological abnormalities in *NDUFAF2*  
6 patients primarily involve the brainstem, cerebellum, upper cervical spinal cord, and basal ganglia  
7 <sup>30</sup>, similar to MRI findings in *MORC2* patients. Infantile-onset brainstem neurodegenerative  
8 disease with early lethality is also the reported phenotype associated with a bi-allelic *ERCC8*-  
9 *NDUFAF2* deletion <sup>42</sup>, further supporting that *NDUFAF2* repression is the major cause of LS in  
10 *MORC2* patients.

11 The *MORC2* epismature was found to be conserved across tissues despite the large differences  
12 in DNA methylation between blood and fibroblasts. To date, DNA methylation epismatures have  
13 mainly been identified and validated in blood samples, with only the Sotos epismature replicated  
14 in fibroblasts on a small sample size <sup>43</sup>. Here, we provide an additional example of epismature  
15 stability across tissues. This cross-tissue stability has the advantage of allowing the performance  
16 of functional studies on different cell lines, including fibroblast cell lines, to assess the effect of  
17 potential treatment options. The conservation of the epismature across tissues raises the question  
18 of when the epismature is established. Correlation between the blood and fibroblast methylation  
19 pattern with the biochemical defects and clinical manifestation affecting different organs argues  
20 that the *MORC2* methylation signature is likely determined early in development.

21 *MORC2* binds to DNA in a non-sequence-specific manner <sup>44</sup>, modulating chromatin structure to  
22 facilitate gene silencing. While a single-gene study has shown that *MORC2* forms a complex with  
23 DNA methyltransferases (DNMTs) at gene promoters to mediate transcription repression <sup>15</sup>, a  
24 systematic analysis of its interactions with DNMTs is still lacking. The promoter hypermethylation  
25 due to *MORC2* mutations observed in this study supports the interaction between *MORC2* and  
26 DNMTs. Further functional studies are needed to clarify the mechanisms by which *MORC2* binds  
27 to gene promoters and interacts with chromatin modifiers such as DNMTs. Of note, not all changes  
28 in gene expression can be directly attributed to promoter hypermethylation. Some of these changes  
29 may be secondary effects mediated by the repression of ZNFs, some of which function as

1 transcription factors and could indirectly influence RNA expression. However, we found no  
2 evidence that any repressed ZNFs regulate any known Mendelian disease genes.

3 How the methylation pattern gets established is beyond the focus of the current study. The  
4 observation of patients with the same mutation but different methylation patterns may reflect a  
5 complex mechanism with a number of components involved in the establishment of the patient-  
6 specific signature. Such variability may stem from random influences, differences in the proteins  
7 involved, or polymorphisms in the target regions. We could not identify any polymorphisms in the  
8 promoter regions of the target genes that were associated with methylation levels, probably due to  
9 the small cohort of patients with the same genotype. A larger cohort would increase the power to  
10 investigate this question.

11 RNA-seq has recently been used as a complementary diagnostic tool to DNA sequencing by  
12 quantifying the direct effects of genetic variants on candidate gene expression and splicing<sup>24,25</sup>.  
13 To our knowledge, the *MORC2* RNA-signature discovered in this study is the first gene-specific  
14 RNA-signature for a monogenic disorder. *MORC2* might not be the only gene where downstream  
15 target genes can be linked to pleiotropic effects. Transcriptome studies from patients with disorders  
16 with known episignatures can indicate whether the observed RNA-signature is unique to *MORC2*  
17 or can be extended to other genes. Screening for RNA-signature could broaden the diagnostic  
18 application of RNA-seq.

19 Episignatures hold significant potential as both therapeutic targets and biomarkers for assessing  
20 treatment efficacy. DNMT inhibitors, such as azacitidine and decitabine, have demonstrated  
21 clinical benefit in certain hematological malignancies<sup>45</sup>. However, their applicability in the  
22 treatment of *MORC2*-related disorders may be limited by their toxicity and off-target effects.  
23 Given the gain-of-function pathomechanism, direct targeting of the *MORC2* disease allele, either  
24 at the RNA level using antisense oligonucleotides (ASOs) or at the protein level with inhibitors  
25 like geldanamycin or radicicol<sup>46,47</sup>, presents another promising therapeutic strategy. Further  
26 research is warranted to evaluate the efficacy of these approaches, both individually and in  
27 combination, in the treatment of *MORC2*-related disorders.

28 The finding of *MORC2* gain-of-function driven DNA methylation accounting for the phenotypic  
29 pleiotropy has implications beyond *MORC2*-related disorders. First, we hypothesize the existence  
30 of disease drivers in other disorders with episignatures, specifically when they are conserved

1 across tissues. Outlier detection may help to identify these drivers. Second, we hypothesize an  
2 epigenetic contribution to other Mendelian disorders with known pleiotropy.

3

## 4 **Data availability**

5 The dataset generated and analyzed in the current study is available on request.

## 6 **Acknowledgements**

7 We are grateful to the families and patients without whom this study would not have been possible.

8

## 9 **Funding**

10 This study was supported by the BMBF (German Federal Ministry of Education and Research)  
11 through the mitoNET German Network for Mitochondrial Diseases (grant number 01GM1906B),  
12 PerMiM Personalized Mitochondrial Medicine (grant number 01KU2016A), the EJP RD project  
13 GENOMIT (01GM1920A, genomit.eu), the German Center for Child and Adolescent Health  
14 (DZKJ) under the funding code 01GL2406B, the Bavarian State Ministry of Health and Care  
15 within its framework of DigiMed Bayern (grant number DMB-1805-0002), and the European  
16 Union's Horizon 2020 research and innovation program project Recon4IMD (grant number  
17 101080997).

18 K.M. acknowledges support from Grant-in-Aid for Research on Measures for Intractable Diseases  
19 (H27-Nanji-Ippan-028) from the Ministry of Health, Labor and Welfare, Japan.

20 K.M., Ya.O., and Yu.O. acknowledge the support from a grant for the Practical Research Project  
21 for Rare/Intractable Diseases from AMED (Fund ID: 23ek0109625, 23ek0109636,  
22 24lk0221189s0301).

23 M.A. and Yu.O. were supported in part by Grant-in-Aid from the Research Committee of Ataxia,  
24 Health Labour Sciences Research Grant, the Ministry of Health, Labour and Health, Welfare and  
25 Labour, Japan (2016100002B). M.A. and Yu.O. acknowledge support from the Japan Agency for  
26 Medical Research and Development (grant numbers 201442014A and 201442071A). M.A. and

1 Yu.O. have also received support from JSPS KAKENHI (grant numbers JP18H02742,  
2 JP20K16604, JP21K15702, JP21H02842, JP22K15713, JP22K07495, JP22K07519,  
3 JP23K06931, and JP23K06966, JP24K18708).

4 M.Z. receives research support from the German Research Foundation (DFG 458949627; ZE  
5 1213/2-1). M.Z. acknowledges grant support from the EJP RD (EJP RD Joint Transnational Call  
6 2022) and the German Federal Ministry of Education and Research (BMBF, Bonn, Germany),  
7 awarded to the project PreDYT (PREdictive biomarkers in DYsTonia, 01GM2302), and from the  
8 Federal Ministry of Education and Research (BMBF) and the Free State of Bavaria under the  
9 Excellence Strategy of the Federal Government and the Länder, as well as by the Technical  
10 University of Munich—Institute for Advanced Study. M.Z.'s research is supported by a  
11 “Schlüsselprojekt” grant from the Else Kröner-Fresenius-Stiftung (2022\_EKSE.185).

12 F.D. was supported by a grant of the German Research Foundation/Deutsche  
13 Forschungsgemeinschaft (DI 1731/2-3) and by a grant from the “Elterninitiative Kinderkrebsklinik  
14 e.V.” (Düsseldorf; #701900167).

15 C.L. is a member of the ERN-NMD and the interERN for mitochondrial disorders.

16 C.S. was supported by the DFG (SCHL2276/2-1, 450149205-TRR333/1).

17

## 18 **Competing interests**

19 The authors declare no conflict of interest.

20

## 21 **Supplementary material**

22 Supplementary material is available at *Brain* online.

23

## 24 **References**

25 1. Thaxton C, Goldstein J, DiStefano M, et al. Lumping versus splitting: How to approach  
26 defining a disease to enable accurate genomic curation. *Cell Genomics*. 2022;2(5):100131.

- 1 doi:10.1016/j.xgen.2022.100131
- 2 2. Albulym OM, Kennerson ML, Harms MB, et al. MORC2 mutations cause axonal Charcot-  
3 Marie-Tooth disease with pyramidal signs. *Ann Neurol.* 2016;79(3):419-427.  
4 doi:10.1002/ana.24575
- 5 3. Ando M, Okamoto Y, Yoshimura A, et al. Clinical and mutational spectrum of Charcot-  
6 Marie-Tooth disease type 2Z caused by MORC2 variants in Japan. *Eur J Neurol.*  
7 2017;24(10):1274-1282. doi:10.1111/ene.13360
- 8 4. Sevilla T, Lupo V, Martínez-Rubio D, et al. Mutations in the MORC2 gene cause axonal  
9 Charcot-Marie-Tooth disease. *Brain J Neurol.* 2016;139(Pt 1):62-72.  
10 doi:10.1093/brain/awv311
- 11 5. Schottmann G, Wagner C, Seifert F, Stenzel W, Schuelke M. MORC2 mutation causes severe  
12 spinal muscular atrophy-phenotype, cerebellar atrophy, and diaphragmatic paralysis. *Brain J*  
13 *Neurol.* 2016;139(Pt 12):e70. doi:10.1093/brain/aww252
- 14 6. Kistol D, Tsygankova P, Krylova T, et al. Leigh Syndrome: Spectrum of Molecular Defects  
15 and Clinical Features in Russia. *Int J Mol Sci.* 2023;24(2):1597. doi:10.3390/ijms24021597
- 16 7. McCormick EM, Keller K, Taylor JP, et al. Expert Panel Curation of 113 Primary  
17 Mitochondrial Disease Genes for the Leigh Syndrome Spectrum. *Ann Neurol.* 2023;94(4):696-  
18 712. doi:10.1002/ana.26716
- 19 8. Stafki SA, Turner J, Littel HR, et al. The Spectrum of MORC2-Related Disorders: A Potential  
20 Link to Cockayne Syndrome. *Pediatr Neurol.* 2023;141:79-86.  
21 doi:10.1016/j.pediatrneurol.2023.01.011
- 22 9. Guillen Sacoto MJ, Tchasovnikarova IA, Torti E, et al. *De Novo* Variants in the ATPase  
23 Module of MORC2 Cause a Neurodevelopmental Disorder with Growth Retardation and  
24 Variable Craniofacial Dysmorphism. *Am J Hum Genet.* 2020;107(2):352-363.  
25 doi:10.1016/j.ajhg.2020.06.013
- 26 10. Tchasovnikarova IA, Timms RT, Douse CH, et al. Hyperactivation of HUSH complex  
27 function by Charcot-Marie-Tooth disease mutation in MORC2. *Nat Genet.* 2017;49(7):1035-  
28 1044. doi:10.1038/ng.3878

- 1 11. Xie HY, Zhang TM, Hu SY, Shao ZM, Li DQ. Dimerization of MORC2 through its C-terminal  
2 coiled-coil domain enhances chromatin dynamics and promotes DNA repair. *Cell Commun*  
3 *Signal.* 2019;17(1):160. doi:10.1186/s12964-019-0477-5
- 4 12. Douse CH, Bloor S, Liu Y, et al. Neuropathic MORC2 mutations perturb GHKL ATPase  
5 dimerization dynamics and epigenetic silencing by multiple structural mechanisms. *Nat*  
6 *Commun.* 2018;9(1):651. doi:10.1038/s41467-018-03045-x
- 7 13. Liu N, Lee CH, Swigut T, et al. Selective silencing of euchromatic L1s revealed by genome-  
8 wide screens for L1 regulators. *Nature.* 2018;553(7687):228-232. doi:10.1038/nature25179
- 9 14. Shao Y, Li Y, Zhang J, et al. Involvement of histone deacetylation in MORC2-mediated down-  
10 regulation of carbonic anhydrase IX. *Nucleic Acids Res.* 2010;38(9):2813-2824.  
11 doi:10.1093/nar/gkq006
- 12 15. Wang T, Qin Z yi, Wen L zhi, et al. Epigenetic restriction of Hippo signaling by MORC2  
13 underlies stemness of hepatocellular carcinoma cells. *Cell Death Differ.* 2018;25(12):2086-  
14 2100. doi:10.1038/s41418-018-0095-6
- 15 16. Emmanuele V, Ganesh J, Vladutiu G, et al. Time to harmonize mitochondrial syndrome  
16 nomenclature and classification: A consensus from the North American Mitochondrial Disease  
17 Consortium (NAMDC). *Mol Genet Metab.* 2022;136(2):125-131.  
18 doi:10.1016/j.ymgme.2022.05.001
- 19 17. Wilson BT, Stark Z, Sutton RE, et al. The Cockayne Syndrome Natural History (CoSyNH)  
20 study: clinical findings in 102 individuals and recommendations for care. *Genet Med.*  
21 2016;18(5):483-493. doi:10.1038/gim.2015.110
- 22 18. Spitz MA, Severac F, Obringer C, et al. Diagnostic and severity scores for Cockayne  
23 syndrome. *Orphanet J Rare Dis.* 2021;16(1):63. doi:10.1186/s13023-021-01686-8
- 24 19. Aryee MJ, Jaffe AE, Corrada-Bravo H, et al. Minfi: a flexible and comprehensive  
25 Bioconductor package for the analysis of Infinium DNA methylation microarrays.  
26 *Bioinformatics.* 2014;30(10):1363-1369. doi:10.1093/bioinformatics/btu049
- 27 20. Houseman EA, Accomando WP, Koestler DC, et al. DNA methylation arrays as surrogate  
28 measures of cell mixture distribution. *BMC Bioinformatics.* 2012;13:86. doi:10.1186/1471-  
29 2105-13-86

- 1 21. Pelegí-Sisó D, de Prado P, Ronkainen J, Bustamante M, González JR. methylclock: a  
2 Bioconductor package to estimate DNA methylation age. *Bioinformatics*. 2021;37(12):1759-  
3 1760. doi:10.1093/bioinformatics/btaa825
- 4 22. Levy MA, Relator R, McConkey H, et al. Functional correlation of genome-wide DNA  
5 methylation profiles in genetic neurodevelopmental disorders. *Hum Mutat*. 2022;43(11):1609-  
6 1628. doi:10.1002/humu.24446
- 7 23. Seczynska M, Bloor S, Cuesta SM, Lehner PJ. Genome surveillance by HUSH-mediated  
8 silencing of intronless mobile elements. *Nature*. 2022;601(7893):440-445.  
9 doi:10.1038/s41586-021-04228-1
- 10 24. Yépez VA, Gusic M, Kopajtich R, et al. Clinical implementation of RNA sequencing for  
11 Mendelian disease diagnostics. *Genome Med*. 2022;14(1):38. doi:10.1186/s13073-022-01019-  
12 9
- 13 25. Kremer LS, Bader DM, Mertes C, et al. Genetic diagnosis of Mendelian disorders via RNA  
14 sequencing. *Nat Commun*. 2017;8(1):15824. doi:10.1038/ncomms15824
- 15 26. Kopajtich R, Smirnov D, Stenton SL, et al. Integration of proteomics with genomics and  
16 transcriptomics increases the diagnostic rate of Mendelian disorders. Published online March  
17 12, 2021:2021.03.09.21253187. doi:10.1101/2021.03.09.21253187
- 18 27. Invernizzi F, D'Amato I, Jensen PB, Ravaglia S, Zeviani M, Tiranti V. Microscale oxygraphy  
19 reveals OXPHOS impairment in MRC mutant cells. *Mitochondrion*. 2012;12(2):328-335.  
20 doi:10.1016/j.mito.2012.01.001
- 21 28. Brechtmann F, Mertes C, Matusėvičiūtė A, et al. OUTRIDER: A Statistical Method for  
22 Detecting Aberrantly Expressed Genes in RNA Sequencing Data. *Am J Hum Genet*.  
23 2018;103(6):907-917. doi:10.1016/j.ajhg.2018.10.025
- 24 29. Douse CH, Tchasovnikarova IA, Timms RT, et al. TASOR is a pseudo-PARP that directs  
25 HUSH complex assembly and epigenetic transposon control. *Nat Commun*. 2020;11(1):4940.  
26 doi:10.1038/s41467-020-18761-6
- 27 30. Abu Hanna F, Zehavi Y, Cohen-Barak E, et al. Lack of mitochondrial complex I assembly  
28 factor NDUFAF2 results in a distinctive infantile-onset brainstem neurodegenerative disease  
29 with early lethality. *Orphanet J Rare Dis*. 2024;19(1):92. doi:10.1186/s13023-024-03094-0

- 1 31. Formosa LE, Dibley MG, Stroud DA, Ryan MT. Building a complex complex: Assembly of  
2 mitochondrial respiratory chain complex I. *Semin Cell Dev Biol.* 2018;76:154-162.  
3 doi:10.1016/j.semcdb.2017.08.011
- 4 32. Hoefs SJG, Dieteren CEJ, Distelmaier F, et al. *NDUFA2* Complex I Mutation Leads to Leigh  
5 Disease. *Am J Hum Genet.* 2008;82(6):1306-1315. doi:10.1016/j.ajhg.2008.05.007
- 6 33. Bertola DR, Cao H, Albano LMJ, et al. Cockayne syndrome type A: novel mutations in eight  
7 typical patients. *J Hum Genet.* 2006;51(8):701-705. doi:10.1007/s10038-006-0011-7
- 8 34. Calmels N, Botta E, Jia N, et al. Functional and clinical relevance of novel mutations in a large  
9 cohort of patients with Cockayne syndrome. *J Med Genet.* 2018;55(5):329-343.  
10 doi:10.1136/jmedgenet-2017-104877
- 11 35. Henning KA, Li L, Iyer N, et al. The Cockayne syndrome group A gene encodes a WD repeat  
12 protein that interacts with CSB protein and a subunit of RNA polymerase II TFIIF. *Cell.*  
13 1995;82(4):555-564. doi:10.1016/0092-8674(95)90028-4
- 14 36. Lee GS, Kwak G, Bae JH, et al. Morc2a p.S87L mutant mice develop peripheral and central  
15 neuropathies associated with neuronal DNA damage and apoptosis. *Dis Model Mech.*  
16 2021;14(10):dmm049123. doi:10.1242/dmm.049123
- 17 37. Gaertner A, Burr L, Klauke B, et al. Compound Heterozygous FKTN Variants in a Patient  
18 with Dilated Cardiomyopathy Led to an Aberrant  $\alpha$ -Dystroglycan Pattern. *Int J Mol Sci.*  
19 2022;23(12):6685. doi:10.3390/ijms23126685
- 20 38. Godfrey C, Escolar D, Brockington M, et al. Fukutin gene mutations in steroid-responsive  
21 limb girdle muscular dystrophy. *Ann Neurol.* 2006;60(5):603-610. doi:10.1002/ana.21006
- 22 39. Sivera R, Lupo V, Frasquet M, et al. Charcot–Marie–Tooth disease due to MORC2 mutations  
23 in Spain. *Eur J Neurol.* 2021;28(9):3001-3011. doi:10.1111/ene.15001
- 24 40. Duan X, Liu X, Wang G, et al. Characterization of genotype–phenotype correlation with  
25 MORC2 mutated Axonal Charcot–Marie–Tooth disease in a cohort of Chinese patients.  
26 *Orphanet J Rare Dis.* 2021;16(1):244. doi:10.1186/s13023-021-01881-7
- 27 41. Kerkhof J, Rastin C, Levy MA, et al. Diagnostic utility and reporting recommendations for  
28 clinical DNA methylation epigenature testing in genetically undiagnosed rare diseases. *Genet*

- 1 *Med.* 2024;26(5):101075. doi:10.1016/j.gim.2024.101075
- 2 42. Sabharwal A, Gupta V, Kv S, et al. Whole genome sequencing followed by functional analysis  
3 of genomic deletion encompassing *ERCC8* and *NDUFAF2* genes in a non-consanguineous  
4 Indian family reveals dysfunctional mitochondrial bioenergetics leading to infant mortality.  
5 *Mitochondrion.* 2024;75:101844. doi:10.1016/j.mito.2024.101844
- 6 43. Choufani S, Cytrynbaum C, Chung BHY, et al. NSD1 mutations generate a genome-wide  
7 DNA methylation signature. *Nat Commun.* 2015;6(1):10207. doi:10.1038/ncomms10207
- 8 44. Fendler NL, Ly J, Welp L, et al. Identification and characterization of a human MORC2 DNA  
9 binding region that is required for gene silencing. *Nucleic Acids Res.* Published online  
10 December 31, 2024:gkae1273. doi:10.1093/nar/gkae1273
- 11 45. Derissen EJB, Beijnen JH, Schellens JHM. Concise Drug Review: Azacitidine and Decitabine.  
12 *The Oncologist.* 2013;18(5):619-624. doi:10.1634/theoncologist.2012-0465
- 13 46. Sharma SV, Agatsuma T, Nakano H. Targeting of the protein chaperone, HSP90, by the  
14 transformation suppressing agent, radicicol. *Oncogene.* 1998;16(20):2639-2645.  
15 doi:10.1038/sj.onc.1201790
- 16 47. Stebbins CE, Russo AA, Schneider C, Rosen N, Hartl FU, Pavletich NP. Crystal Structure of  
17 an Hsp90–Geldanamycin Complex: Targeting of a Protein Chaperone by an Antitumor Agent.  
18 *Cell.* 1997;89(2):239-250. doi:10.1016/S0092-8674(00)80203-2

19

## 20 **Figure legends**

21 **Figure 1 Phenotypic heterogeneity in MORC2-related disorders.** (A), Main phenotypic  
22 abnormalities observed in MORC2-related disorders are shown. (B), Donut chart showing the  
23 distribution of different disorders associated with MORC2 pathogenic variants in a total of 112  
24 patients, including both previously reported patients ( $n = 73$ ) and new patients reported in this  
25 paper ( $n = 39$ ). (C), Lollipop plot showing the distribution of pathogenic variants in MORC2 and  
26 their associated disorders. Variants reported more than 5 times or associated with more than one  
27 disorder are labeled in the plot. The data includes 112 patients described in panel B.

28

1 **Figure 2 Tissue-independent *MORC2*-specific epesignature are mainly localized in gene**  
2 **promoters. (A)**, Volcano plot of differential methylation analysis comparing *MORC2* patients ( $n$   
3 = 10) to healthy controls ( $n = 46$ ). Shown in blue and red are the 760 significantly differentially  
4 methylated CpGs with a Bonferroni-adjusted  $p$ -value threshold of  $< 0.05$ . **(B)**, The mean of  
5 methylation Z-score of 220 CpGs (*MORC2* epesignature) (y-axis) was calculated for each  
6 individual with blood DNA methylation. Every dot presented one individual. The controls (grey  
7 dots) consist of healthy individuals ( $n = 58$ ) and patients with mutations in other genes than  
8 *MORC2* ( $n = 424$ ). The yellow point shows the individual with a benign stopgain variant in  
9 *MORC2* (p.Arg90Ter), and the cannon pink dots represent the *MORC2* patients. **(C)**, Result of the  
10 SVM classifier trained on blood DNA methylation of 220 CpGs to predict *MORC2* patients. The  
11 y-axis shows the probability that the DNA methylation profile matches the *MORC2*-specific  
12 epesignature. Each dot represents one individual, and the x-axis indicates the causal genes or  
13 groups. "Mitochondrial": Patients with pathogenic variants in MD genes ( $n = 301$ ).  
14 "MORC2\_Benign": Two patients with benign missense variants in *MORC2*. "MORC2\_LOF":  
15 One patient with a benign LOF variant in *MORC2*. Training Set: Blood DNA methylation of 10  
16 *MORC2* patients and 46 controls. Test Set: Blood DNA methylation of three *MORC2* patients, 12  
17 controls, one MORC2\_Benign, 367 patients with other genetic disorders, and fibroblast DNA  
18 methylation of six *MORC2* patients, four controls, and 14 patients with MD. Validation Set: Blood  
19 DNA methylation of 22 *MORC2* patients, 20 patients with other genetic disorders, and fibroblast  
20 DNA methylation of 6 *MORC2* patients and one patient with another genetic disorder. **(D)**,  
21 Localization of the 760 CpGs identified in panel A relative to gene structure and known *MORC2*  
22 target sites. "Body" refers to CpG sites located within gene bodies and 3' untranslated regions (3'  
23 UTRs). "TSS" denotes the transcription start site. "TSS200" represents CpG sites located 0–200  
24 bases upstream of the TSS, and "TSS1500" represents CpG sites located 200–1500 bases upstream  
25 of the TSS. Fisher's exact test showed significant enrichment of differentially methylated CpG  
26 sites. **(E)**, Venn diagram illustrating the overlap among CpG sites located in promoter regions,  
27 *MORC2* binding sites, and HUSH target sites. Out of the 760 differentially methylated CpG sites,  
28 463 that belong to at least one of these categories are included in the diagram. SVM: support vector  
29 machine, MD: mitochondrial disease, LOF: loss-of-function.

30

1 **Figure 3 *MORC2*-specific RNA-signature in fibroblast cell lines.** (A), Volcano plot of  
 2 differential expression analysis in fibroblast cell lines comparing *MORC2* patients ( $n = 10$ ) to  
 3 healthy or diseased controls ( $n = 42$ ). 106 significant differentially expressed genes at a Benjamin  
 4 Hochberg-adjusted  $p$ -value threshold of  $< 0.05$  are shown in blue and red. (B), Result of the SVM  
 5 classifier trained on the expression profile of 106 genes, identified in panel A. The y-axis shows  
 6 the probability that the transcriptome profile matches the *MORC2*-specific RNA-signature.  
 7 Training Set: 10 *MORC2* patients, 13 healthy controls, 29 diseased controls. Test Set: Two  
 8 *MORC2* patients, five healthy controls, five diseased controls, and 168 genetically undiagnosed  
 9 patients. SVM: support vector machine.

10  
 11 **Figure 4 The downstream effect of aberrant DNA methylation on gene expression.** (A), Mirror  
 12 Manhattan plot displaying the results of differential methylation analysis (top panel, red dots) and  
 13 differential expression analysis (bottom panel, blue dots). The y-axis represents  $-\log_{10}(p\text{-value})$  for  
 14 both analyses, and the x-axis denotes the genomic positions of CpG sites or genes. Threshold  $p$ -  
 15 values were set at  $7.93 \times 10^{-8}$  (corresponding to Bonferroni-adjusted  $p$ -value  $< 0.05$ ) for differential  
 16 methylation and  $2.7 \times 10^{-4}$  (corresponding to Benjamin Hochberg-adjusted  $p$ -value  $< 0.05$ ) for  
 17 differential expression analyses (indicated by dashed lines). Differentially methylated CpG sites  
 18 mapped to C2H2-ZNF genes and differentially expressed C2H2-ZNF genes are highlighted in  
 19 green. Genes that are both differentially methylated and differentially expressed are shown in bold  
 20 shape. OMIM disease genes that are both differentially methylated and expressed are enclosed in  
 21 rectangles and labeled. The Venn diagram at the bottom illustrates the overlap between C2H2-  
 22 ZNFs, HUSH target genes (Seczynska et al., 2022), differentially expressed genes, and  
 23 differentially methylated genes. (B), Enrichment of C2H2-ZNFs among both differentially  
 24 methylated CpGs (top) and differentially expressed genes (bottom) with Fisher's exact test  $p$ -  
 25 values of  $1.35 \times 10^{-146}$  and  $3.18 \times 10^{-40}$ , respectively. OMIM: Online Mendelian Inheritance in  
 26 Man, ZNFs: zinc finger genes.

27  
 28 **Figure 5 Hypermethylation and downregulation of disease-associated genes by *MORC2* gain-  
 29 of-function variants.** (A), LocusZoom plot for *ERCC8* and *NDUFAF2* genes based on the  
 30 differential methylation analysis (from Fig. 2A). Each dot represents a CpG site, and the y-axis

1 indicates the  $-\log_{10}(p\text{-value})$  of the differential methylation analysis. **(B)**, Promoter methylation  
 2 and expression levels of *ERCC8* and *NDUFAF2* in *MORC2* patients and controls. The mean  
 3 methylation (*y-axis* of the left panel) represents the average of the methylation level (beta value)  
 4 across 14 CpGs located in the *ERCC8-NDUFAF2* promoter region. The right panels display RNA  
 5 Z-scores derived from OUTRIDER results for *ERCC8* and *NDUFAF2* expression levels,  
 6 respectively. **(C)**, NDUFAF2 protein levels in *MORC2* patients and controls. The left panel shows  
 7 protein Z-scores of NDUFAF2 derived from PROTRIDER results. The middle panel shows the  
 8 mitochondrial respiratory chain complex I with significant recurrent protein outliers (protein Z-  
 9 score  $< -2$ ) in *MORC2* patients highlighted and named in red (one-sided Fisher's exact test  $p\text{-value}$   
 10  $< 0.05$ ). The number of *MORC2* patients in whom the protein was identified as an outlier is written  
 11 in brackets. Proteins shown in grey were either not detected or not significant. The right panel  
 12 shows the mitochondrial respiration rate in control and *MORC2* patients with CMT or LS.  $P\text{-values}$   
 13 were computed using an independent two-sample *t*-test. **(D)**, LocusZoom plot for the *FKTN* gene  
 14 based on the differential methylation analysis (from Fig 2A). Promoter methylation and expression  
 15 levels of *FKTN* in *MORC2* patients and controls are shown, respectively. The mean methylation  
 16 represents the average of the methylation level (beta value) across 7 CpG sites located in the *FKTN*  
 17 promoter region. **(E)**, LocusZoom plot for *SDHAF4* gene-based based on the differential  
 18 methylation analysis (from Fig 2A). The promoter methylation level of *SDHAF4* in *MORC2*  
 19 patients with measured mitochondrial respiratory chain complex II activity and controls are shown  
 20 (middle panel). *MORC2* patients with complex II deficiency are indicated by rectangles. The mean  
 21 methylation represents the average of the methylation level (beta value) across 8 CpGs located in  
 22 the *SDHAF4* promoter. The correlation between the level of promoter methylation and the  
 23 expression (RNA Z-score) is shown (right panel). The dashed line in the locusZoom plots  
 24 represents the  $p\text{-value}$  threshold of  $7.93 \times 10^{-8}$ , corresponding to a Bonferroni-adjusted  $p\text{-value}$   $<$   
 25  $0.05$ . *MORC2* binding sites (Tchasovnikarova et al., 2017) and HUSH target sites (Seczynska et  
 26 al., 2022) are shown as green rectangles and double-sided arrows in the locusZoom plots,  
 27 respectively. CMT: Charcot-Marie-Tooth disease, LS: Leigh syndrome.

28

29 **Figure 6 The phenotypic spectrum of *MORC2*-related disorder can be explained by DNA**  
 30 **methylation.** **(A)**, Stacked bar plot showing the distribution of HPO terms in our in-house *MORC2*  
 31 patients with clinical diagnoses of CMT or MD. The *x-axis* represents the fraction of patients with

1 a clinical diagnosis of CMT or MD exhibiting specific phenotypic abnormalities. Only HPO terms  
2 reported in at least 40% of patients within each category are displayed. **(B)**, MDS plot based on  
3 blood DNA methylation of 80 phenotype-specific DMPs. The size of each point reflects the  
4 Cockayne syndrome radiological score, with larger points indicating a greater resemblance of  
5 patients' phenotype to CS. The dataset includes *MORC2* patients with CMT phenotype ( $n = 26$ ),  
6 *MORC2* patients with MD ( $n = 8$ ), and controls ( $n = 58$ ). **(C)**, The methylation level of *ERCC8*  
7 and *NDUFAF2* promoter in controls and *MORC2* patients with a clinical diagnosis of CMT or  
8 MD in blood and fibroblast. The *y-axis* represents the average methylation level (beta value) of 14  
9 CpGs mapped to the *ERCC8-NDUFAF2* promoter. *P-values* were computed using an independent  
10 two-sample *t-test*. Patients with LS are included in the category of MD. The variants associated  
11 with different phenotypes are labeled in panels B and C. **(D)**, Scaled density plots of the mean  
12 DNA methylation Z-scores of hypermethylated CpGs identified in EWAS, selected as *MORC2*  
13 epismature, identified as phenotype specific, and located in *ERCC8-NDUFAF2* promoter. The  
14 dataset includes blood or fibroblast DNA methylation of 466 healthy or diseased controls, 27  
15 *MORC2* patients with CMT, and 19 *MORC2* patients with MD. *P-values* were computed to  
16 compare the level of DNA methylation between the *MORC2* patients with CMT and MD using an  
17 independent two-sample *t-test*. HPO: Human Phenotype Ontology, CMT: Charcot-Marie-Tooth  
18 disease, MD: mitochondrial disease, LS: Leigh syndrome.

19  
20  
21

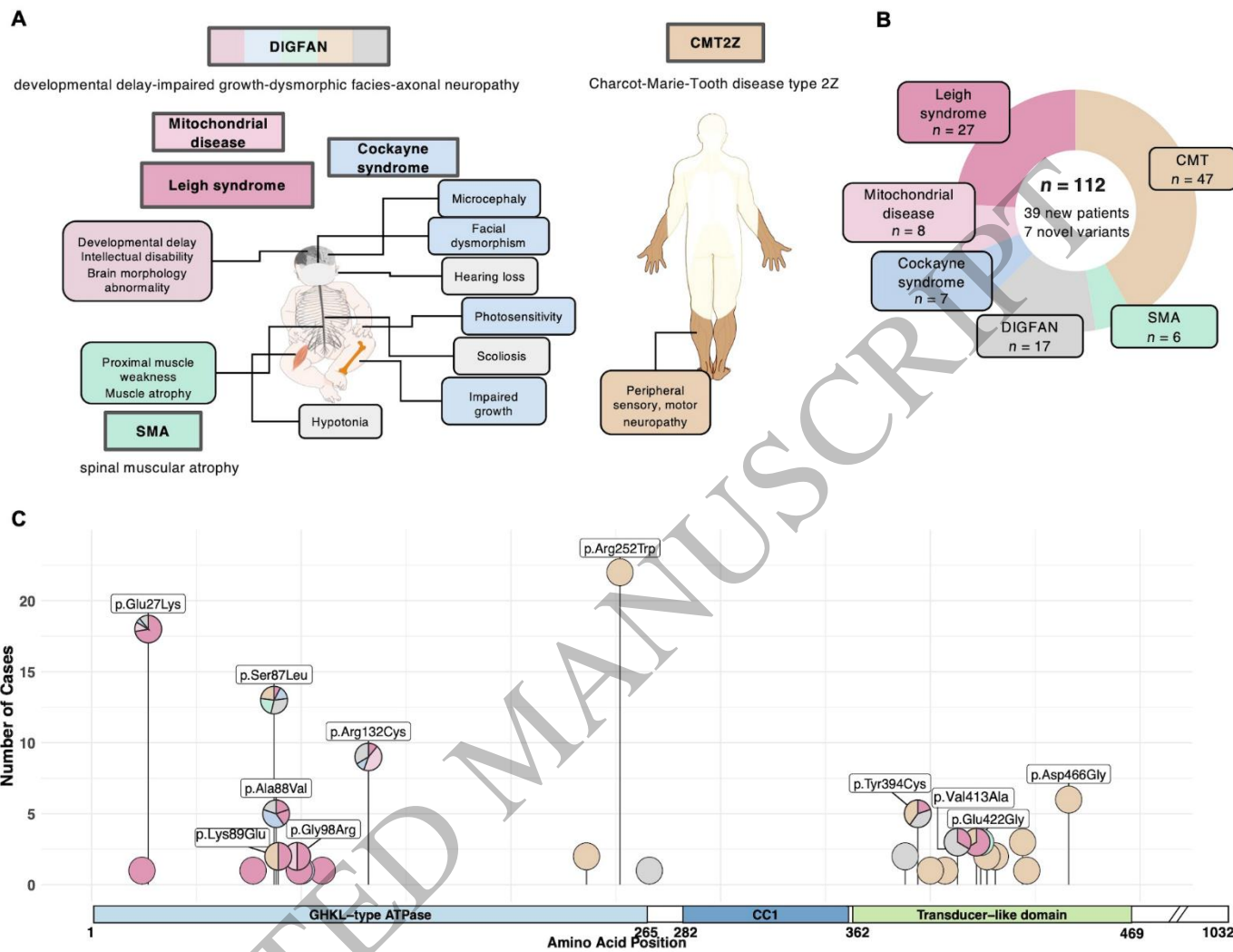


Figure 1  
184x144 mm (x DPI)

1  
2  
3  
4

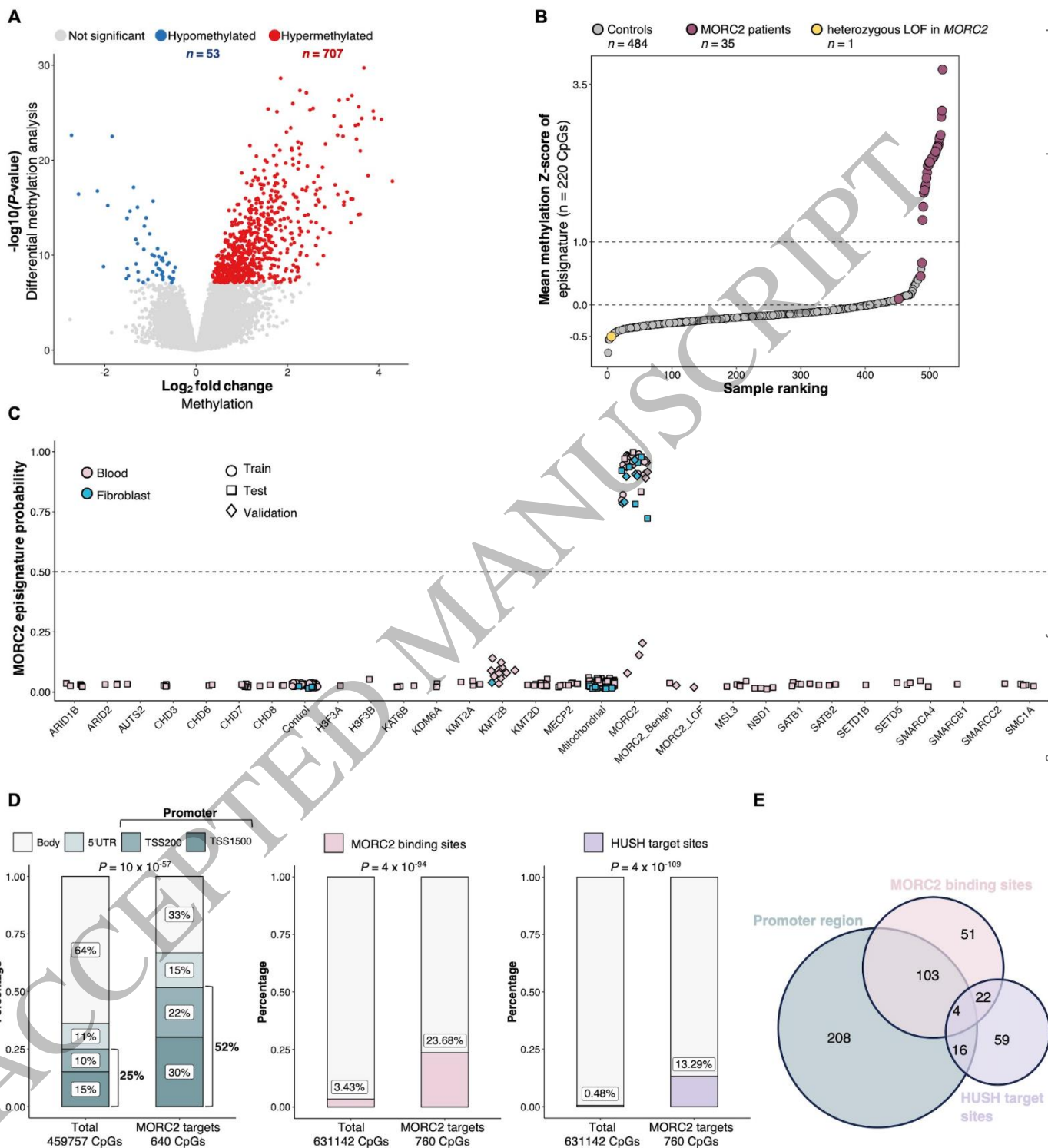


Figure 2  
185x202 mm (x DPI)

1  
2  
3  
4



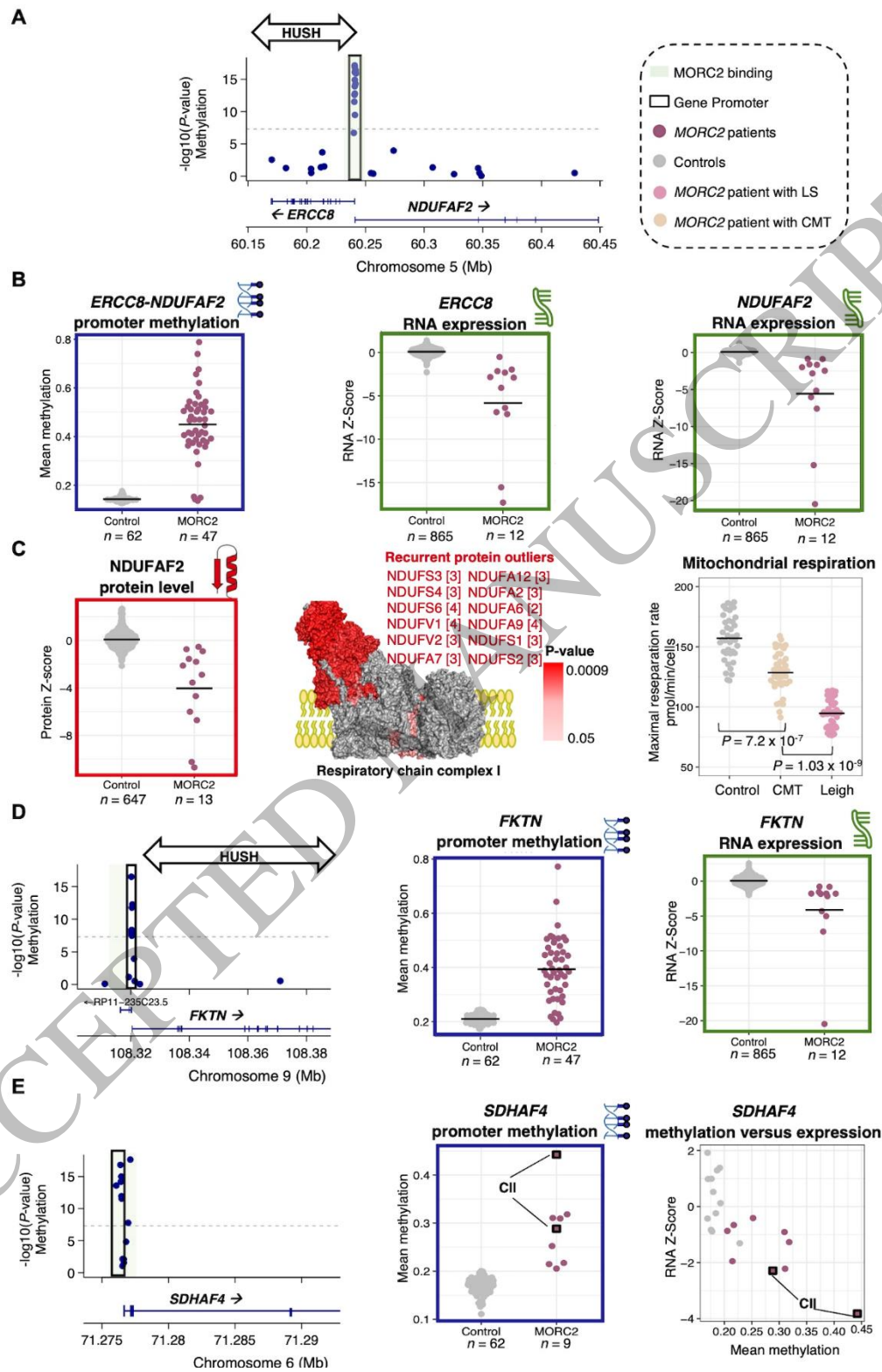


Figure 5  
132x208 mm (x DPI)

1  
2  
3  
4

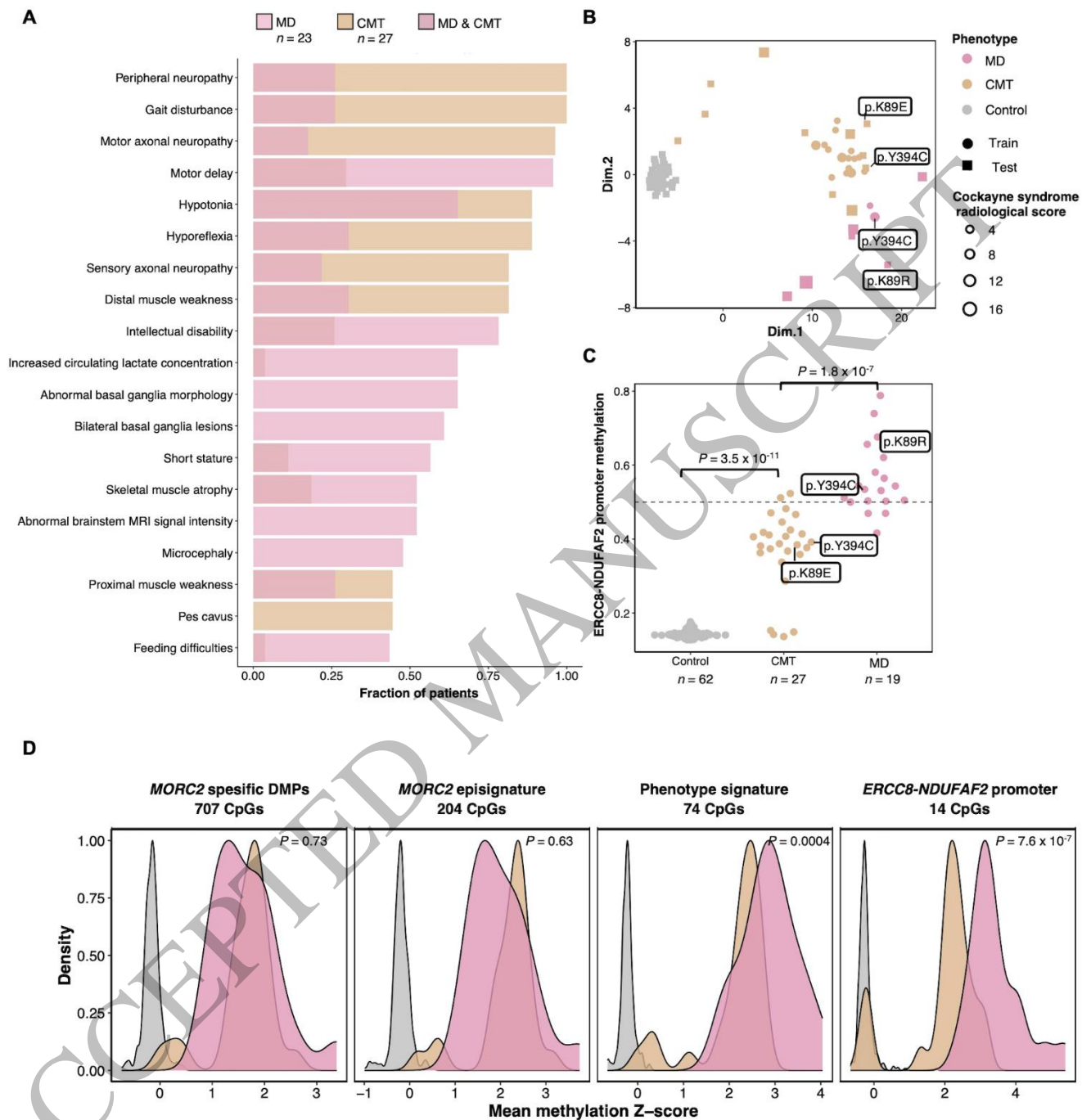


Figure 6  
177x181 mm (x DPI)

1  
2  
3